Homogeneous water nucleation in a laminar flow diffusion chamber

Alexandra A. Manka,[1,a)] David Brus,[2,3] Antti-Pekka Hyvärinen,[2] Heikki Lihavainen,[2] Judith Wölk,[1] and Reinhard Strey[1]
[1]*Institut für Physikalische Chemie, Universität zu Köln, Luxemburger Str. 116, 50939 Köln, Germany*
[2]*Finnish Meteorological Institute, Erik Palménin aukio 1, P.O. Box 503, FI-00101 Helsinki, Finland*
[3]*Laboratory of Aerosol Chemistry and Physics, Institute of Chemical Process Fundamentals, Academy of Sciences of the Czech Republic, Rozvojová 135, CZ-165 02 Prague 6, Czech Republic*

(Received 27 January 2010; accepted 15 April 2010; published online 23 June 2010)

Homogeneous nucleation rates of water at temperatures between 240 and 270 K were measured in a laminar flow diffusion chamber at ambient pressure and helium as carrier gas. Being in the range of 10^2-10^6 cm^{-3} s^{-1}, the experimental results extend the nucleation rate data from literature consistently and fill a pre-existing gap. Using the macroscopic vapor pressure, density, and surface tension for water we calculate the nucleation rates predicted by classic nucleation theory (CNT) and by the empirical correction function of CNT by Wölk and Strey [J. Phys. Chem. B **105**, 11683 (2001)]. As in the case of other systems (e.g., alcohols), CNT predicts a stronger temperature dependence than experimentally observed, whereas the agreement with the empirical correction function is good for all data sets. Furthermore, the isothermal nucleation rate curves allow us to determine the experimental critical cluster sizes by use of the nucleation theorem. A comparison with the critical cluster sizes calculated by use of the Gibbs–Thomson equation is remarkably good for small cluster sizes, for bigger ones the Gibbs–Thomson equation overestimates the cluster sizes. © *2010 American Institute of Physics*. [doi:10.1063/1.3427537]

I. INTRODUCTION

Water, the most important substance for life, can be found in nature in several phases, e.g., gaseous steam, liquid water, and different kinds of solid ice. The phase transitions between these states have been under investigation for over a hundred years[1] but how they take place is, up to date, not totally understood. The first step in almost any first-order phase transition is nucleation, i.e., the formation of the first, initial fragments, or clusters of the new phase out of the mother phase. Nucleation and, in particular, condensation of water take place in many industrial processes and play a major role in the atmosphere. Cloud formation and its impact on climate change are still poorly understood. Therefore it is of great interest to clarify the physics of water nucleation in order to make accurate predictions for the condensation process. In the past century homogeneous nucleation of liquid droplets from water vapor in the absence of any foreign particles or surfaces has been investigated as a function of supersaturation S and temperature T using a variety of experimental devices.[2] These devices include supersonic nozzles (SSNs),[3,4] shock tubes,[5] cloud chambers,[6–8] nucleation pulse chambers (NPCs),[9,10] and flow diffusion chambers.[11,12] Combining the measuring windows for all devices, nearly 20 orders of magnitude in nucleation rate J, which is the number of nuclei formed per unit time and per unit volume, can be covered.[13] Nevertheless, there are still areas where less data are available. In order to complete the present data we studied homogeneous nucleation of water in a laminar flow diffusion chamber (LFDC).[12,14,15] The homogeneous nucleation rates were measured for four different nucleation temperatures (240, 250, 260, and 270 K), under ambient pressure and with helium as carrier gas. We compare our data with theoretical predictions such as classical nucleation theory[16] (CNT) and the empirical correction function for CNT by Wölk and Strey,[17] as well as with experimental data measured by other groups in different devices.[11,17–25] Obtaining isothermal nucleation rates as a function of supersaturation S enables us to determine the experimental critical cluster sizes (the excess number of molecules in the critical clusters) as a function of temperature according to Kashchiev[26–28] from the slopes of the J versus S isotherms. Furthermore, we compare the experimental critical cluster sizes to cluster sizes calculated by use of the classical Gibbs–Thomson equation and to cluster sizes available from literature.[11,17–25]

II. EXPERIMENT

A. Principle of operation

The general experimental setup of the LFDC used in this study was developed by Lihavainen and Viisanen[12] and can be found in detail elsewhere. Here, just a brief overview of the working principle of the LFDC and the experimental procedure is given.

The LFDC mainly consists of three parts: the saturator, the preheater, and the condenser, each separately temperature controlled. A steady flow of helium (AGA, Finland, purity 99.9999%) as carrier gas is brought into the saturator, a reservoir half filled with liquid water, and gets fully saturated with water vapor. The amount of water [ULTRAPURE, Millipore, USA, Total Organic Carbon less than 10 ppb (ppb denotes parts per 10^9), resistivity 18.2 MΩ cm at 25 °C]

[a)]Electronic mail: alexandra.manka@uni-koeln.de.

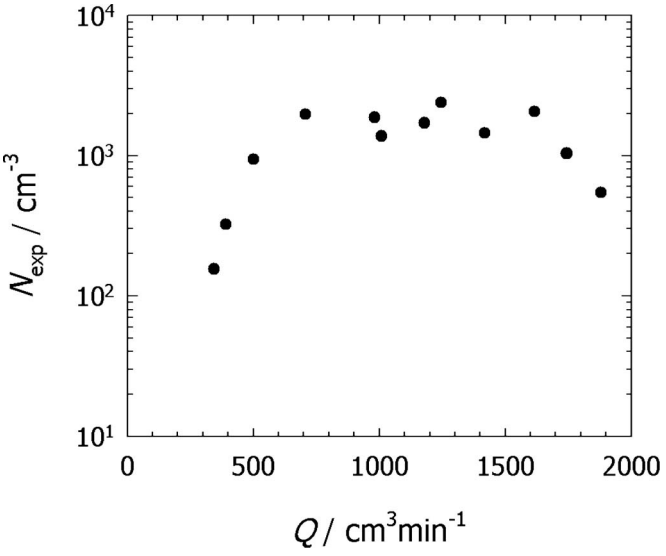

FIG. 1. The number of counted particles N_{exp} as a function of the flow rate Q in the LFDC.

evaporating and saturating the carrier gas flow is controlled by the temperature of the saturator T_{sat}. Then, the vapor-gas mixture flows through the preheater and enters the condenser, which consists of two coaxial vertical tubes with same inner diameter. In the preheater, kept at higher temperature T_{pre} as the saturator ($T_{pre} > T_{sat}$), a laminar flow with a known velocity profile is achieved. Furthermore, the boundary conditions and the initial temperature (T_{pre}) of the mixture are defined. Entering the condenser, which is at a much lower temperature T_{con} than the saturator ($T_{con} < T_{sat}$), the stream is rapidly cooled, leading to an increase in the saturation ratio S of the vapor. If the achieved supersaturation exceeds a critical value, nucleation occurs. Since the mixture still remains supersaturated while flowing through the condenser, the formed particles can grow to droplets of optically detectable size. At the end of the condenser the droplets are counted by light scattering with a TSI 3010 condensation particle counter's optical head. To ensure a stable and well measurable particle flow, we tested the dependency of the particle number concentration N_{exp} on the flow rate of the gas mixture Q (see Fig. 1).

According to the mathematical model[12] the nucleation rate, and therefore the particle number concentration N_{exp}, should be independent of the flow at higher flow rates. However, if the flow rate is too high, the residence time in the saturator is too short for full saturation of the flow. Hence the saturation ratio is lower than expected and the nucleation rate drops drastically. At lower flow rates the nucleation rate is reduced by several effects arising from the heat and mass transfer relations and due to vapor depletion. Longer residence time in the nucleation zone leads to an increased condensational growth of the freshly nucleated particles and a faster self-quenching process of nucleation. To avoid both effects the flow rate was set to ~ 1000 cm^3 min^{-1} (~ 17 cm^3 s^{-1}) for this investigation. Another important aspect when conducting experiments with the LFDC is that the heat transfer by conduction must be higher than the mass transfer by diffusion. Then, the equilibrium vapor pressure decreases faster than the actual vapor pressure, the saturation ratio rises and a well defined nucleation zone can be achieved. Therefore the Lewis number Le, which is the ratio of the rates of heat transfer by conduction and mass transfer by diffusion,

$$Le = \frac{k}{D\rho C_p}, \tag{1}$$

where k is the thermal conductivity of the vapor-carrier gas mixture, D is the binary diffusion coefficient, ρ is the density of the mixture, and C_p is the heat capacity of the mixture, should be higher than unity. The Lewis numbers for water in helium are 2.05 at 270 K and 2.14 at 240 K.

B. Experimental procedure

All measurements were performed under atmospheric pressure and with helium as carrier gas. To measure one nucleation rate isotherm, the temperatures of the preheater T_{pre} and the condenser T_{con} were kept constant, while the temperature of the saturator T_{sat} was varied to achieve different saturation ratios. Once the temperatures were stabilized, a flow of helium was introduced into the system and the volume flow rate Q was set to ~ 17 cm^3 s^{-1}. Simultaneously, we started to record the particle concentration N_{exp} and measured the temperatures T_{pre}, T_{con}, T_{sat}, and the laboratory temperature T_{lab} as well as the total pressure p_{tot} in the device, which is the same as atmospheric pressure. For 0.5–3 min the particle concentration remained stable and well measurable, after that time interval it dropped drastically because the water started to freeze at the walls in the tube and decreased the inner diameter, and also changed the boundary conditions. At that point we stopped the measurement and started to deice and dry the tube. Therefore we heated the tube up to 30 °C and flushed it with hot air (~ 400 K) for 30 min. Before starting a new measurement we adjusted the condenser to the desired temperature while flushing the tube backward via optical head, condenser, and preheater with dry argon to avoid any condensation on the inner walls. When the desired temperature of the condenser was reached we started a new measurement.

C. Data analysis

Direct measuring of any physical conditions inside the tube is not possible without disturbing the flow. Therefore a mathematical model developed by Lihavainen and Viisanen[12] and corrected by Brus *et al.*[29] was used to determine the profiles of temperature T, vapor pressure of the water vapor p_{vap}, equilibrium vapor pressure p_{eq}, supersaturation S (which is the ratio of the actual vapor pressure over the equilibrium vapor pressure), and nucleation rate according to CNT J_{theo} along the z-axis at the center of the condenser tube. This model bases on the equations for heat and mass transfer, equations of motion, and the equation of continuity. The thermodynamic data used for the evaluation of the profiles are summarized in Ref. 23 except for the density of liquid water which was taken from Ref. 19. The profiles itself are shown in Fig. 2.

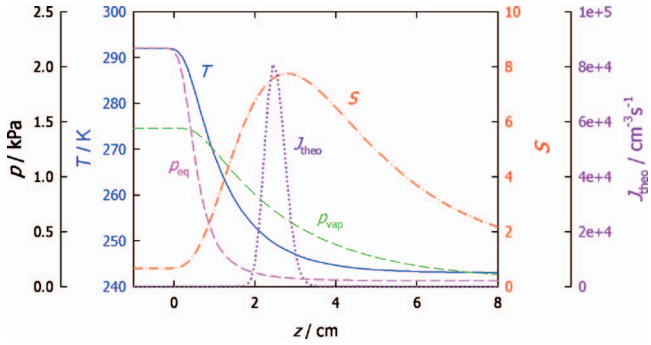

FIG. 2. The temperature T, equilibrium vapor pressure p_{eq}, vapor pressure of water vapor p_{vap}, supersaturation S, and calculated nucleation rate J_{theo} profiles along the length of the condenser z. The flow rate of the gas mixture is 17 cm^3 s^{-1}.

As the temperature and therefore the equilibrium vapor pressure drops dramatically whereas the actual vapor pressure decreases much slower, the supersaturation rises and nucleation occurs. The calculated nucleation rate maximum is located slightly before the supersaturation maximum because nucleation is a strong function of both temperature and supersaturation. After nucleation the vapor still remains supersaturated and the nucleated particles are able to grow to droplets of optically detectable size.

Nucleation occurs in a narrow region at the center of the condenser. The grown particles are counted at the end of the condenser while flowing through the particle counter and given in units of successfully nucleated particles per unit time formed in the entire chamber volume. Anyhow, this value does not account for the exact volume in which the particles have been formed. Therefore we need to convert these results into conventional nucleation rates in units of cm^{-3} s^{-1}, where the volume is limited to the exact nucleation region in the chamber. To calculate the maximum experimental nucleation rate J_{exp}^{max}, which is defined as the onset of nucleation, we use the following relationship by Wagner and Anisimov:[30]

$$\frac{J_{exp}^{max}}{\int J_{exp} dV} = \frac{J_{theo}^{max}}{\int J_{theo} dV}. \tag{2}$$

Here, J_{theo}^{max} is the theoretical nucleation rate maximum for the nucleation conditions in the condenser, $\int J_{theo} dV$ is the theoretical nucleation rate integrated over the entire volume of the condenser, and $\int J_{exp} dV$ is the measured particle number concentration N_{exp} in cm^{-3} multiplied by the flow rate. This relationship bases on the fact that experimental and theoretical nucleation rates usually have same slopes while they differ in the absolute values.[17,31,32] For the sake of simplicity, in this study we used CNT (Ref. 16),

$$J_{CNT} = \sqrt{\frac{2\sigma}{\pi m}} v_l \left(\frac{p_{vap}}{k_B T}\right)^2 \exp\left[-\frac{16\pi v_l^2 \sigma^3}{3(k_B T)^3 (\ln S)^2}\right], \tag{3}$$

where σ is the surface tension, m is the molecular mass, v_l is the volume of one liquid molecule, p_{vap} is the vapor pressure, k_B is the Boltzmann constant, T is the temperature, and S is the supersaturation ratio. Former studies showed that by use of different theories the calculated experimental results for J_{exp}^{max} do not change by more than 10%–50%.[33] Since the onset of nucleation has been defined as the point where nucleation reaches its maximum J_{max}, the exact nucleation conditions such as the temperature, pressure, and supersaturation are denoted as T_{Jmax}, p_{Jmax}, and S_{Jmax}, respectively, and can be obtained from the profiles directly.

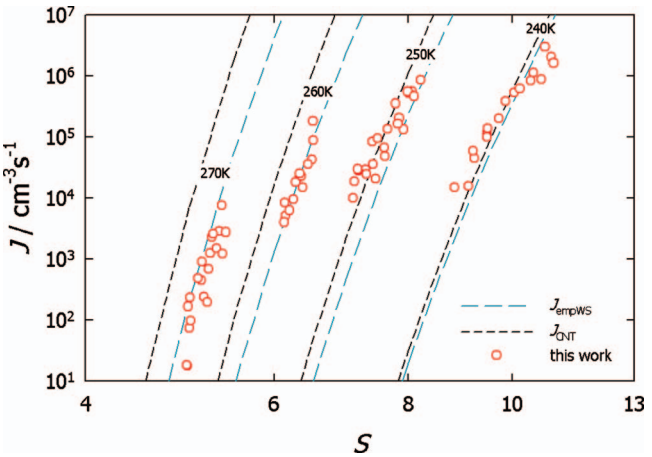

FIG. 3. The measured isothermal homogeneous nucleation rates of water J (circles) as a function of supersaturation S in comparison with predictions of CNT J_{CNT} (short dashed lines) and the empirical correction function for CNT by Wölk and Strey (Ref. 17) J_{empWS} (long dashed lines).

III. RESULTS AND DISCUSSION

A. Nucleation rates

We measured homogeneous nucleation rates J of condensing water vapor in the LFDC at 240, 250, 260, and 270 K at ambient atmospheric pressure and with helium as carrier gas as a function of supersaturation. The conditions at which the theoretical nucleation rate reaches its maximum J_{max} were determined from the profiles inside the tube. The experimental data such as the nucleation temperature T_{Jmax} and the saturation ratio S_{Jmax} at these theoretical nucleation rate maxima as well as the measured nucleation rates J_{exp} are available in electronic form on the Supplementary Material repository.[34] The measured isothermal nucleation rates as a function of supersaturation in comparison with predictions by CNT and the empirical correction function for CNT by Wölk and Strey[17] are shown in Fig. 3.

The agreement of our experimental results with CNT predictions at 240 and 250 K seems to be good, but going to higher temperatures such as 260 and 270 K, the experimental and theoretical results start to diverge. CNT predicts too high nucleation rates and deviations up to two orders of magnitude occur, although the slopes of the measured and the calculated isotherms remain the same. This wrong temperature dependence of CNT was already found and analyzed by Wölk and Strey[17] and Wölk *et al.*[32] and accounted for with the empirical correction function,

$$J_{exp} = J_{CNT} \exp\left(A + \frac{B}{T}\right), \tag{4}$$

where parameters A and B are given as $A=-27.56$ and $B=6500$ K, respectively. To calculate this expression they used different thermophysical expressions for the equilib-

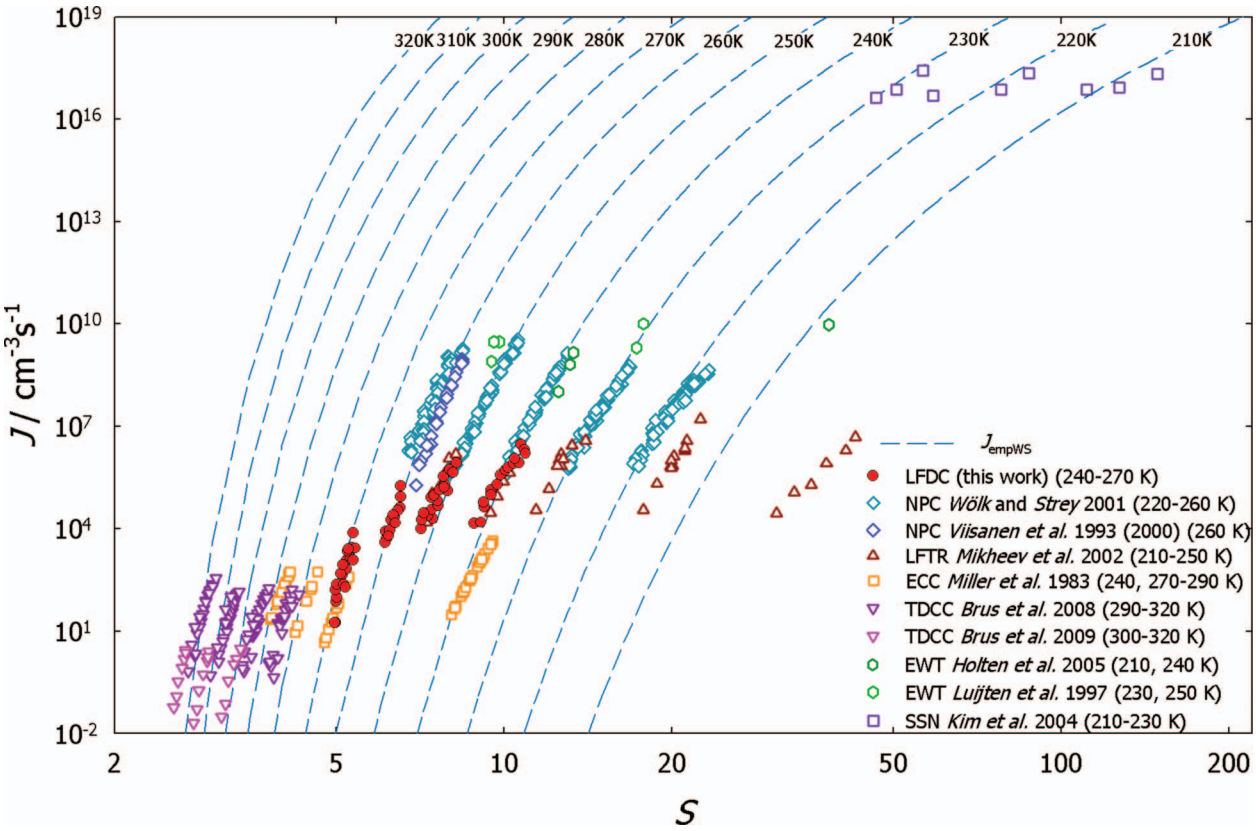

FIG. 4. Comparison of all available experimental homogeneous nucleation rate data for water J as a function of supersaturation S at 210–320 K (References 11, 17–23, and 25) in 10 K steps with the empirical correction function for CNT by Wölk and Strey (Ref. 17) J_{empWS} (dashed lines).

rium vapor pressure and the liquid density as we did to analyze the experimental data (see Sec. II C). Therefore we compared both expressions for vapor pressure[17,23] and density[17,19] in the temperature range of interest (210–320 K) and found a difference of less than 1%, respectively.

The comparison of our experimental data with the correction function reveals a good agreement at all measured temperatures (Fig. 3). At 240 and 250 K the predictions by CNT and the correction function are very similar; at 260 and 270 K the correction function predicts lower rates than CNT and therefore agrees with the experimental results. An overall comparison of our data with nucleation rates measured in different devices such as the laminar flow tube reactor (LFTR) (upward triangles),[11] the NPC (diamonds),[17–19] the expansion wave tube (EWT) (hexagons),[20,21] the expansion cloud chamber (ECC) (pale rectangles),[22] the thermal diffusion cloud chamber (TDCC) (downward triangles),[23,24] and the SSN (dark rectangles),[25] as well as with nucleation rates calculated by use of the correction function for CNT (J_{empWS}, dashed lines) is summarized in Fig. 4. Altogether, the nucleation rates measured in all these devices cover 20 orders of magnitude and a temperature range of 210–320 K.

Our LFDC data extend the NPC data which are the basis of the correction function to lower rates. Furthermore there is a slight overlap with the NPC data in the 240 and 250 K isotherms. We also find a rather good agreement with the LFTR data by Mikheev *et al.*[11] at these temperatures and at 270 K our data coincide with the ECC data by Miller *et al.*[22] The overall agreement with the empirical correction function for CNT is astonishing good for all data sets, even at very high nucleation rates like in the SSN. Some deviations can be found by taking a closer look at the data measured at very low temperatures and at high temperatures. For the nucleation rates measured in the LFTR by Mikheev *et al.*[11] the agreement with the correction function is also good at 230–250 K, but looking at lower temperatures such as 220 K significant discrepancies from two, and for 210 K up to five orders of magnitude occur. At 280 and 290 K the predictions by the empirical function are too high by up to two orders of magnitude compared to data measured in the ECC by Miller *et al.*[22] Looking at the data measured in the TDCC altogether, the slopes of the isotherms are not as steep as predicted by theory. For the TDCC data measured in Prague, Czech Republic, by Brus *et al.*[23] in 2008, the empirical correction function overestimates the rates by up to two orders of magnitude at 290 and 300 K, for higher temperatures, such as 310 and 320 K, the agreement becomes better but the slopes of the isotherms are still flatter than predicted. In contrast, comparing the TDCC data measured in Marburg, Germany, by Brus *et al.*[24] in 2009 to the correction function, here the correction function underestimates the nucleation rate between 300 and 320 K by up to two orders of magnitude with highest discrepancies at highest temperatures.

There are also other theories, models, and empirical functions available to predict nucleation rates but since the predictions by CNT or alternatively the empirical correction function for CNT are rather good, we resign from other comparisons. Recent theories represent the Reguera–Reiss

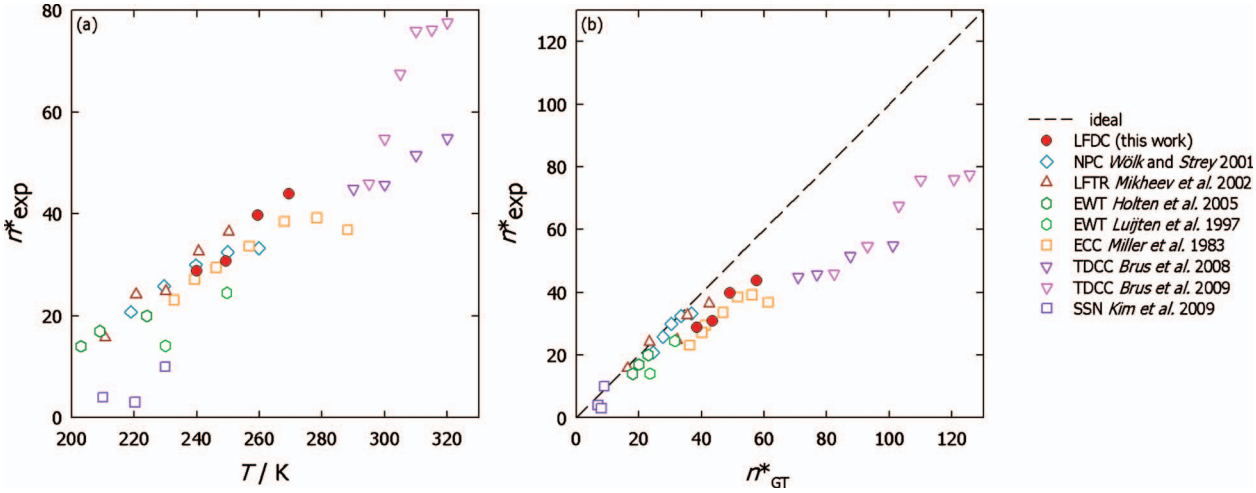

FIG. 5. (a) The experimentally determined critical cluster sizes n^*_{exp} for the series of literature data (Refs. 11, 17–23, and 25) as a function of temperature T. (b) Comparison of n^*_{exp} with the critical cluster sizes determined by use of the Gibbs–Thomason equation n^*_{GT}. The dashed line represents perfect agreement.

theory[35,36] or the mean-field kinetic nucleation theory by Kalikmanov,[37] which still need to be tested, but calculating nucleation rates with these models is much more complicated than by use of CNT. The scaled nucleation model by Hale[38–40] bears very similar results as the empirical correction function by Wölk and Strey[17] and therefore we omit this comparison. Another empirical correction function by Holten *et al.*[20] is very simple to calculate but only valid within the temperature range of 200–240 K and nucleation range of $3\times10^{7-11}$ cm^{-3} s^{-1}.

B. Critical cluster sizes

By use of the nucleation theorem[26]

$$n^*_{exp} \approx \left(\frac{\partial \ln J}{\partial \ln S}\right)_T, \tag{5}$$

we were able to determine the molecular content of the critical clusters n^*_{exp} from the slopes of the measured J versus S isotherms. These critical cluster sizes as a function of the isothermal temperature T show a uniform, linear increase with increasing temperature for all data sets [see Fig. 5(a)]. Our data fit rather well in this trend.

The classical way to calculate the critical cluster size is by use of the Gibbs–Thomson equation[17,41]

$$n^*_{GT} = \frac{32\pi}{3}\frac{v_l^2\sigma^3}{(k_BT\ln S)^3}. \tag{6}$$

A comparison of the critical cluster sizes determined with both methods is summarized in Fig. 5(b).

The Gibbs–Thomson equation seems to predict the critical cluster size quite well for very small cluster sizes and the agreement is rather good for $n^*<40$. However, at larger critical cluster sizes ($n^*>40$), or likewise higher temperatures, the agreement gets worse like for the cluster sizes determined by Brus *et al.*[23,24] Here, the Gibbs–Thomson clusters get too large by up to a factor of 2. Considering the capillarity approximation utilized to calculate the size of the Gibbs–Thomson clusters this finding is surprising since the classical approach should work better at bigger cluster sizes and worse for smaller ones.

IV. CONCLUSION

In this work the experimental data for the homogeneous nucleation of water measured in the LFTR by Mikheev *et al.*[11] could be reproduced and extended by measurements in a LFDC. Some of literature data measured in other devices[11,17–23,25] could also be reproduced and the gap between nucleation rates in the range of $10^3<J$ cm^{-3} s$^{-1}<10^6$ at temperatures between 240 and 270 K could be closed effectively (see Fig. 4). Compared to predictions by CNT,[16] the disparate temperature trend of CNT has been confirmed, while the slope of the measured nucleation rate versus supersaturation curve can be predicted properly. The empirical correction function for CNT by Wölk and Strey[17] accounts for this disparate temperature trend and agrees with our data consistently and also with most other data. Only at very high and very low temperatures small discrepancies can be found. From the slopes of the measured isotherms the experimental critical cluster sizes have been determined and compared to calculations by use of the Gibbs–Thomson equation.[17,41] At small critical cluster sizes the agreement is good but looking at higher temperatures and therefore bigger critical clusters, the Gibbs–Thomson equation starts to overestimate their size. This finding is surprising since the physical properties used to calculate the critical cluster size originate from the bulk phase and should work better for bigger cluster sizes.

ACKNOWLEDGMENTS

The travel and accommodation expenses for this project were financially supported by ACCENT, Atmospheric Composition Change, The European Network of Excellence in the program "Access to Infrastructures" and the DAAD, German Academic Exchange Service. FCoE (Finnish Center

of Excellence of Academy of Finland—Physics, Chemistry and Biology of Atmospheric Composition and Climate Change) projects are also greatly acknowledged for financial support.

[1] C. R. T. Wilson, Philos. Trans. R. Soc. London, Ser. A **189**, 871 (1897).
[2] R. H. Heist and H. J. He, J. Phys. Chem. Ref. Data **23**, 781 (1994).
[3] P. P. Wegener, in *Gas Dynamics*, edited by P. P. Wegener (Dekker, New York, 1966).
[4] B. E. Wyslouzil, G. Wilemski, M. G. Beals, and M. B. Frish, Phys. Fluids **6**, 2845 (1994).
[5] F. Peters, Exp. Fluids **1**, 143 (1983).
[6] J. L. Katz and B. J. Ostermier, J. Chem. Phys. **47**, 478 (1967).
[7] R. H. Heist, M. Janjua, and J. Ahmed, J. Chem. Phys. **98**, 4443 (1994).
[8] J. Smolík and V. Ždímal, Aerosol Sci. Technol. **20**, 127 (1994).
[9] P. E. Wagner and R. Strey, J. Phys. Chem. **85**, 2694 (1981).
[10] R. Strey, P. E. Wagner, and Y. Viisanen, J. Phys. Chem. **98**, 7748 (1994).
[11] V. B. Mikheev, P. M. Irving, N. S. Laulainen, S. E. Barlow, and V. V. Pervukhin, J. Chem. Phys. **116**, 10772 (2002).
[12] H. Lihavainen and Y. Viisanen, J. Phys. Chem. B **105**, 11619 (2001).
[13] K. Iland, J. Wedekind, J. Wölk, P. E. Wagner, and R. Strey, J. Chem. Phys. **121**, 12259 (2004).
[14] A.-P. Hyvärinen, H. Lihavainen, Y. Viisanen, and M. Kulmala, J. Chem. Phys. **120**, 11621 (2004).
[15] D. Brus, A.-P. Hyvärinen, V. Ždímal, and H. Lihavainen, J. Chem. Phys. **122**, 214506 (2005).
[16] R. Becker and W. Döring, Ann. Phys. **24**, 719 (1935).
[17] J. Wölk and R. Strey, J. Phys. Chem. B **105**, 11683 (2001).
[18] Y. Viisanen, R. Strey, and H. Reiss, J. Chem. Phys. **112**, 8205 (2000).
[19] Y. Viisanen, R. Strey, and H. Reiss, J. Chem. Phys. **99**, 4680 (1993).
[20] V. Holten, D. G. Labetski, and M. E. H. van Dongen, J. Chem. Phys. **123**, 104505 (2005).
[21] C. C. M. Luijten, K. J. Bosschaart, and M. E. H. van Dongen, J. Chem. Phys. **106**, 8116 (1997).
[22] R. C. Miller, R. J. Anderson, J. L. Kassner, J. Hagen, and D. E. Hagen, J. Chem. Phys. **78**, 3204 (1983).
[23] D. Brus, V. Ždímal, and J. Smolík, J. Chem. Phys. **129**, 174501 (2008).
[24] D. Brus, V. Ždímal, and H. Uchtmann, J. Chem. Phys. **131**, 074507 (2009).
[25] Y. J. Kim, B. E. Wyslouzil, G. Wilemski, J. Wölk, and R. Strey, J. Phys. Chem. **108**, 4365 (2004).
[26] D. Kashchiev, J. Chem. Phys. **76**, 5098 (1982).
[27] D. W. Oxtoby and D. Kashchiev, J. Chem. Phys. **100**, 7665 (1994).
[28] R. K. Bowles, R. McGraw, P. Schaaf, B. Senger, J.-C. Voegel, and H. Reiss, J. Chem. Phys. **113**, 4524 (2000).
[29] D. Brus, A.-P. Hyvärinen, V. Ždímal, and H. Lihavainen, J. Chem. Phys. **128**, 079901 (2008).
[30] P. E. Wagner and M. P. Anisimov, J. Aerosol Sci. **24**, S103 (1993).
[31] C. Hung, M. J. Krasnopoler, and J. L. Katz, J. Chem. Phys. **90**, 1856 (1989).
[32] J. Wölk, R. Strey, C. H. Heath, and B. E. Wyslouzil, J. Chem. Phys. **117**, 4954 (2002).
[33] K. Hämeri, M. Kulmala, E. Krissinel, and G. Kodenyov, J. Chem. Phys. **105**, 7683 (1996).
[34] See supplementary material at http://dx.doi.org/10.1063/1.3427537 for experimental data.
[35] D. Reguera and H. Reiss, J. Phys. Chem. B **108**, 19831 (2004).
[36] D. Reguera and H. Reiss, Phys. Rev. Lett. **93**, 165701 (2004).
[37] V. I. Kalikmanov, J. Chem. Phys. **124**, 124505 (2006).
[38] B. N. Hale, Phys. Rev. A **33**, 4156 (1986).
[39] B. N. Hale, Metall. Trans. A **23**, 1863 (1992).
[40] B. N. Hale, J. Chem. Phys. **122**, 204509 (2005).
[41] M. Volmer, *Kinetik der Phasenbildung* (Steinkopff, Dresden, 1939).